

Phenomenology of Dark Matter annihilation into a long-lived intermediate state

Ira Z. Rothstein,^{1,*} Thomas Schwetz,^{2,†} and Jure Zupan^{3,4,‡}

¹*Carnegie Mellon University, Dept. of Physics, Pittsburgh PA 15213, USA*

²*Max-Planck-Institute for Nuclear Physics,
PO Box 103980, 69029 Heidelberg, Germany*

³*Theory Division, Physics Department,
CERN, CH-1211 Geneva 23, Switzerland*

⁴*Faculty of mathematics and physics, University of Ljubljana,
Jadranska 19, 1000 Ljubljana, Slovenia*

Abstract

We propose a scenario where Dark Matter (DM) annihilates into an intermediate state which travels a distance $\lambda \equiv v/\Gamma$ on the order of galactic scales and then decays to Standard Model (SM) particles. The long lifetime disperses the production zone of the SM particles away from the galactic center and hence, relaxes constraints from gamma ray observations on canonical annihilation scenarios. We utilize this set up to explain the electron and positron excesses observed recently by PAMELA and ATIC. While an explanation in terms of usual DM annihilations seems to conflict with gamma ray observations, we show that within the proposed scenario, the PAMELA/ATIC results are consistent with the gamma ray data. The distinction from decay scenarios is discussed and we comment on the prospects for DM production at LHC.

*Electronic address: izr@andrew.cmu.edu

†Electronic address: schwetz@mpi-hd.mpg.de

‡Electronic address: jure.zupan@cern.ch

I. INTRODUCTION

An exciting and very plausible possibility is that dark matter (DM) interacts non-gravitationally. A very active ongoing program exists to search for such interactions both directly and indirectly. Indirect evidence could arise from cosmic ray signals originating from areas of high dark matter density — the galactic halos and cores. Decaying or annihilating DM can act as an additional source of cosmic ray fluxes on Earth, and could be seen as an excess above the expected flux. The channel in which the excess could show up depends on how DM couples to standard model (SM) particles.

DM decays and annihilations into charged particles inevitably lead to enhanced gamma ray fluxes due to internal and final state bremsstrahlung. In both cases the gamma ray spectrum will be correlated with the energy spectrum of charged particle, and will be the same (up to overall energy scale) for the same final states. However, the angular distribution of gamma rays in the sky will differ between the two cases. Since the annihilation rate scales with ρ^2 (ρ being the DM density), the gamma ray signal will be more highly peaked toward the galactic center due to the rise in the density profile for small r . The decay rate, on the other hand, scales linearly with ρ and therefore the gamma ray signal is less peaked.

In this paper we consider an alternative scenario, where the DM annihilates into long lived particles (LLP). This setup will lead to a gamma ray signature which can interpolate between the signatures of DM decays and annihilation. The prolonged decay lifetime of LLP effectively smears out the distribution of gamma rays. To be concrete we will consider this scenario in the context of DM explanation of the positron excess found by PAMELA [1] and ATIC [2]. The PAMELA experiment which sees a rise in the positron-to-electron ratio in cosmic rays for energies between 10 and 100 GeV corroborates and extends the range of earlier data [3], while ATIC sees a rise and then a striking fall near 800 GeV in the power-law for the combined electron and positron flux. The rise at lower energies, below the bump, corroborates previous data [4] while the bump at 800 GeV had never been seen before. Although it seems quite reasonable to believe that this data has an explanation in terms of nearby young pulsars [5, 6, 7, 8, 9, 10, 11, 12] (or some of the data could be spurious), it will serve as a useful tool in highlighting the features of the LLP scenario. In particular, the data exemplify a case where there is a need for an increased annihilation cross section $\langle\sigma v\rangle \sim 10^{-22} \text{ cm}^3/\text{s}$ (relative to the typical cross section $\langle\sigma v\rangle \sim 3 \times 10^{-26} \text{ cm}^3/\text{s}$ needed for $\Omega_{\text{DM}} \sim 0.2$), while there is no evidence of excess in the gamma ray flux in the direction of the galactic center. Standard annihilation scenarios with such large cross sections seem to conflict [13, 14, 15, 16] with the results from the HESS telescope [17, 18] for commonly assumed DM profiles. We will show that, by allowing the annihilation products to be long lived, the constraints from gamma rays can be avoided.

To be specific, let us consider the situation where a DM particle χ annihilates into an intermediate state ϕ which subsequently decays into standard model particles

$$\chi\chi \rightarrow \phi\phi \rightarrow 2 \text{ SM } 2 \overline{\text{SM}}. \quad (1)$$

As an example we will assume in the following that ϕ decays into muons,

$$\phi \rightarrow \mu^+ \mu^-, \quad (2)$$

though our arguments do not rely on the specific decay mode of ϕ . We concentrate on this mode since it is the relevant one for the PAMELA/ATIC data. In contrast to [20, 21, 22,

23, 24, 25] we now assume that ϕ is a long-lived particle (LLP), such that it will propagate over galactic distances.¹ For the moment we will not concern ourselves with whether or not the DM particle χ is a thermal relic. We will return to this issue at the end of the paper in section IV. In Sec. II we present a general discussion of the LLP scenario and discuss the effects on the production of Standard Model particles from DM annihilations focusing on gamma rays. In Sec. III we apply this idea to the recent data from PAMELA and ATIC and show that they can be made consistent with gamma ray observations from HESS even for rather cuspy DM profiles.

II. GAMMA RAYS FROM DM ANNIHILATIONS VIA A LONG-LIVED STATE

A. General discussion

Let a ϕ be produced at $\vec{r} = 0$. Then the probability that it decays in a volume element d^3r around \vec{r} is

$$\frac{1}{4\pi\lambda} \frac{e^{-r/\lambda}}{r^2} d^3r, \quad \text{with} \quad \lambda \equiv \frac{\gamma\beta}{\Gamma} \quad (3)$$

where Γ is the decay rate of ϕ , λ the corresponding decay length in the laboratory frame, while the velocity of ϕ in the laboratory frame, $\beta = v/c$, and the relativistic gamma factor are

$$\gamma = \frac{E_\phi}{m_\phi} = \frac{m_\chi}{m_\phi}, \quad \beta = \frac{p_\phi}{E_\phi} = \sqrt{1 - \frac{1}{\gamma^2}} = \sqrt{1 - \frac{m_\phi^2}{m_\chi^2}}, \quad (4)$$

where $m_{\chi,\phi}$ are the masses of χ and ϕ . In the last equalities above we used the fact that χ is non-relativistic.

Let us now calculate the photon flux resulting from final state radiation of the process shown in Eqs. 1 and 2. The differential photon flux Φ_γ in a solid angle $\Delta\Omega$ is given by

$$\frac{d\Phi_\gamma}{dE_\gamma} = 2 \langle\sigma v\rangle \int_{\Delta\Omega} d\Omega \int_{\text{l.o.s.}} ds \int d^3r' \frac{1}{2} \frac{\rho^2(r')}{m_\chi^2} \frac{1}{4\pi\lambda} \frac{e^{-|\vec{r}-\vec{r}'|/\lambda}}{|\vec{r}-\vec{r}'|^2} \frac{1}{2\pi} \frac{d^2N_\gamma}{dE_\gamma d\cos\theta}. \quad (5)$$

Here $\rho(r)$ is the energy density of DM particles χ , $\langle\sigma v\rangle$ is the averaged annihilation cross section of χ , and we have assumed that χ is a Majorana particle, a choice we shall adopt throughout this work. The factor of $1/2$ accounts for the fact that the incoming particles are identical, as it has not been included in the definition of $\langle\sigma v\rangle$. $d^2N_\gamma/(dE_\gamma d\cos\theta)$ is the double differential gamma spectrum per ϕ decay. It can be obtained by boosting the isotropic spectrum in the ϕ rest frame (RF), where

$$\left. \frac{d^2N_\gamma}{dE_\gamma d\cos\theta} \right|_{\text{RF}} = \left. \frac{1}{2} \frac{dN_\gamma}{dE_\gamma} \right|_{\text{RF}}. \quad (6)$$

The factor 2 in Eq. 5 accounts for the fact that we will have two ϕ decays per annihilation.

¹ Phenomenologically, annihilations into rapidly decaying particles are challenging to distinguish from pure annihilation [16, 26] and thus we will not consider them distinct in this paper.

In Eq. 5 we use coordinates with the origin at the galactic center, and $\chi\chi$ annihilate at the point \vec{r}' and ϕ decays at \vec{r} . Then θ is the angle between the line of sight (l.o.s.) and the direction of motion of ϕ :

$$\cos \theta = -\frac{\hat{s} \cdot (\vec{r} - \vec{r}')}{|\vec{r} - \vec{r}'|} \quad (7)$$

where \hat{s} is the unit vector along the line of sight. In the following we are going to compare the predicted photon flux to data from the HESS telescope, using observations of the galactic center (GC) [17] within a cone of solid angle 10^{-5} . In this case we have

$$\Delta\Omega_{\text{GC}} = 2\pi(1 - \cos \Delta\psi) = 10^{-5}, \quad \int_{\Delta\Omega} d\Omega = \int_0^{2\pi} d\varphi \int_0^{\Delta\psi} \sin \psi d\psi, \quad (8)$$

$$r = \sqrt{r_\odot^2 + s^2 - 2r_\odot s \cos \psi}, \quad \hat{s} = (\cos \psi, \cos \varphi \sin \psi, \sin \varphi \sin \psi), \quad (9)$$

where $r_\odot \simeq 8.5$ kpc is the distance of the solar system from the galactic center. Furthermore, we use the HESS observation of the galactic ridge (GR) [18]. This is a rectangular region of the sky with galactic latitude and longitude of $|l| \leq \Delta l = 0.8^\circ$, $|b| \leq \Delta b = 0.3^\circ$, where the inner region corresponding to the GC defined above has been subtracted. For the GR we have

$$\Delta\Omega_{\text{GR}} \approx 4\Delta l \Delta b - \Delta\Omega_{\text{GC}} \approx 2.8 \times 10^{-4}, \quad \int_{\Delta\Omega} d\Omega \approx 4 \int_0^{\Delta l} dl \int_0^{\Delta b} db, \quad (10)$$

$$r = \sqrt{r_\odot^2 + s^2 - 2r_\odot s \cos l \cos b}, \quad \hat{s} \approx \left(1 - \frac{l^2 + b^2}{2}, l, b\right). \quad (11)$$

Before we specialize to the case of non-relativistic ϕ and proceed with our discussion we mention briefly some limiting cases of Eq. 5. First, we consider the limit $\Gamma \rightarrow \infty$ (or $\lambda \rightarrow 0$). In this case the integrand in Eq. 5 will be non-zero only for $\vec{r} = \vec{r}'$. Hence we can replace $\rho(r') \rightarrow \rho(r)$, which can be pulled out of the d^3r' integral. Using for the remaining d^3r' integral

$$\int d\Omega' \frac{1}{2\pi} \frac{d^2 N_\gamma}{dE_\gamma d\cos \theta} = \frac{dN_\gamma}{dE_\gamma}, \quad (12)$$

one obtains

$$\left. \frac{d\Phi_\gamma}{dE_\gamma} \right|_{\Gamma \rightarrow \infty} = \frac{\langle \sigma v \rangle}{4\pi} \frac{dN_\gamma}{dE_\gamma} \int_{\Delta\Omega} d\Omega \int_{\text{l.o.s.}} ds \frac{\rho^2(r)}{m_\chi^2}. \quad (13)$$

As expected we recover the standard expression for the bremsstrahlung photon flux from annihilation $\chi\chi \rightarrow \ell^+\ell^- + n\gamma$, apart from a factor 2, since in our case there are twice as many photons because of two ϕ decays per χ annihilation (see Eq. 2).

Second, we consider the case of highly relativistic ϕ . Then one has $\gamma \gg 1$ and $\beta \approx 1$, while the photons are collimated with ϕ within an opening angle of size $1/\gamma$. This implies that there is only a contribution to the integral when $(\vec{r} - \vec{r}')$ is aligned with the line of sight, and the d^3r' integration reduces to another integration along the line of sight:

$$\begin{aligned} \left. \frac{d\Phi_\gamma}{dE_\gamma} \right|_{\text{relat.}} &= \frac{\langle \sigma v \rangle}{4\pi} \frac{dN_\gamma}{dE_\gamma} \int_{\Delta\Omega} d\Omega \int_0^\infty ds' \int_0^{s'} ds \frac{\rho^2(r')}{m_\chi^2} \frac{e^{-(s'-s)/\lambda}}{\lambda} \\ &= \frac{\langle \sigma v \rangle}{4\pi} \frac{dN_\gamma}{dE_\gamma} \int_{\Delta\Omega} d\Omega \int_{\text{l.o.s.}} ds' \frac{\rho^2(r')}{m_\chi^2} \left(1 - e^{-s'/\lambda}\right) \end{aligned} \quad (14)$$

As a reference, we also give the expression for the photon flux from decaying dark matter (see, e.g. [19])

$$\left. \frac{d\Phi_\gamma}{dE_\gamma} \right|_{\text{decay}} = \frac{\Gamma}{4\pi} \frac{dN_\gamma}{dE_\gamma} \int_{\Delta\Omega} d\Omega \int_{\text{l.o.s.}} ds \frac{\rho(r)}{m_\chi}, \quad (15)$$

where Γ is the DM decay width. The important difference between decaying and annihilating DM is that the DM density enters linearly in the first case, and quadratically in the second, which has important observational implications discussed below.

B. The effective DM profile for non-relativistic intermediate state ϕ

In order to simplify the calculations we specialize from now on to the case of non-relativistic ϕ , as the generic effects will not change for the case of a relativistic ϕ . The effect of an intermediate LLP with a suitable decay length λ will always be to flatten out the distribution of SM particle production with respect to the DM distribution, independently of its γ . This follows from the structure of Eq. 14 or the general expression Eq. 5. The general case would deserve a dedicated quantitative study which is beyond the scope of the present work.

For non-relativistic ϕ one has $\gamma \approx 1$, $\beta \ll 1$, and the decay of ϕ is isotropic. In particular, the photon spectrum is given by Eq. 6. The spectrum can be pulled out of the integration and the effect is a smearing of the density distribution on the scale λ . One may define an effective density distribution:

$$\begin{aligned} \rho_{\text{eff}}^2(r) &= \int d^3r' \rho^2(r') \frac{1}{4\pi\lambda} \frac{e^{-|\vec{r}-\vec{r}'|/\lambda}}{|\vec{r}-\vec{r}'|^2} \\ &= \frac{1}{2\lambda r} \int_0^\infty dr' r' \rho^2(r') \left[\text{Ei} \left(-\frac{r+r'}{\lambda} \right) - \text{Ei} \left(-\frac{|r-r'|}{\lambda} \right) \right], \end{aligned} \quad (16)$$

with the exponential integral

$$\text{Ei}(x) \equiv -\text{PV} \left(\int_{-x}^\infty dt \frac{e^{-t}}{t} \right). \quad (17)$$

Using the effective DM profile in Eq. 16 we can write the photon flux from a given solid angle $\Delta\Omega$ as

$$\frac{d\Phi_\gamma}{dE_\gamma} = \frac{\langle\sigma v\rangle}{4\pi} \frac{r_\odot \rho_\odot^2}{m_\chi^2} \frac{dN_\gamma}{dE_\gamma} J \Delta\Omega \quad (18)$$

where the dimensionless J -factor is defined by

$$J = \frac{1}{\Delta\Omega} \int_{\Delta\Omega} d\Omega \int_{\text{l.o.s.}} \frac{ds}{r_\odot} \frac{\rho_{\text{eff}}^2(r)}{\rho_\odot^2}. \quad (19)$$

For the numerical calculations in this work we use $\rho_\odot = 0.3 \text{ GeV cm}^{-3}$ and $r_\odot = 8.5 \text{ kpc}$, and for the DM density $\rho(r)$ we always assume a NFW profile [27]

$$\rho(r) = \rho_\odot \frac{r_\odot}{r} \left(\frac{1+r_\odot/r_s}{1+r/r_s} \right)^2, \quad (20)$$

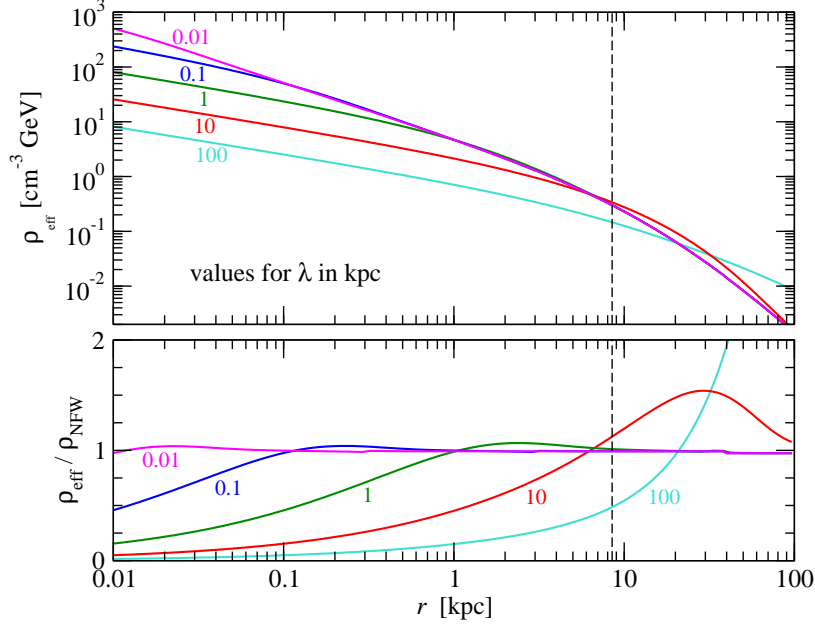


FIG. 1: Upper panel: effective DM density profiles as defined in Eq. 16 for various values of λ . Lower panel, effective DM profiles relative to the NFW profile (corresponding to $\lambda = 0$).

with $r_s = 20$ kpc. Eq. 18 has the same form as the photon flux from standard annihilations $\chi\chi \rightarrow \mu^+\mu^- + n\gamma$, apart from a factor 2 from the decay of two ϕ 's, as mentioned above.

In the non-relativistic case the two parameters m_ϕ and Γ appear only in the particular combination $\lambda = \gamma\beta/\Gamma$, see Eqs. 3 and 4. Therefore, apart from the two parameters $\langle\sigma v\rangle$ and m_χ of the standard annihilation scenario, we have now effectively one additional parameter corresponding to the decay length of ϕ in the rest frame of the galaxy. Numerically one has

$$\lambda = \frac{\gamma\beta}{\Gamma} \approx \frac{\sqrt{2\delta}}{\Gamma} \approx 1.4 \text{ kpc} \left(\frac{\delta}{0.01} \right)^{1/2} \left(\frac{\tau}{10^{12} \text{ s}} \right), \quad (21)$$

with $\delta \equiv (m_\chi - m_\phi)/m_\chi \ll 1$ and $\tau = 1/\Gamma$.

In the LLP scenario the source of SM particles from DM annihilations is proportional to $\rho_{\text{eff}}^2(r)$, while in the case of standard annihilations it is proportional to $\rho^2(r)$. This means that via the propagation of the intermediate state ϕ over galactic distances we decouple to some extent the production of SM particles and associated gammas from the DM distribution. Fig. 1 shows the effective DM profile for various values of λ . From the figure we find that for $r \lesssim \lambda$ we suppress $\rho_{\text{eff}}(r)$ with respect to $\rho(r)$ since the ϕ had no time to decay yet, while for $r \gtrsim \lambda$ we obtain a ρ_{eff} slightly larger than the original DM profile. The relative size of this over-production increases with λ . Finally, at large distances $r \gg \lambda$ all ϕ 's have decayed and we recover the NFW profile.

One can understand this behavior qualitatively from the definition of ρ_{eff} in Eq. 16. From the first line of this equation it follows that for $r \gg \lambda$ the exponential is non-zero only for $\vec{r} \approx \vec{r}'$ and one obtains $\rho_{\text{eff}}(r) \rightarrow \rho(r)$. On the other hand, for $r \ll \lambda$ and for profiles

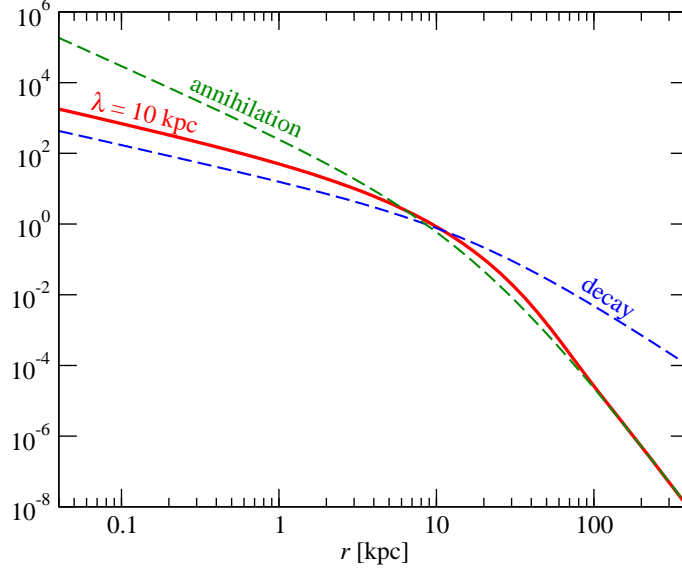


FIG. 2: Interpolation between the SM particle source terms for DM annihilation and decay. The dashed curves show $\rho_{\text{NFW}}^2(r)/\rho_{\odot}^2$ for annihilation and $\rho_{\text{NFW}}(r)/\rho_{\odot}$ for decay, whereas the solid curve corresponds to $\rho_{\text{eff}}^2(r)/\rho_{\odot}^2$ for DM annihilation into a long lived intermediate state with a decay length of $\lambda = 10$ kpc.

λ [kpc]	0	1	10	100
GC	14200	781	101	10.4
GR	2000	468	70	7.7

TABLE I: J -factors for GC and GR for various values of λ .

$\rho(r) \propto r^{-\gamma}$ ($\gamma \gtrsim 1$) one has roughly

$$\rho_{\text{eff}}^2(r)|_{r \ll \lambda} \propto \int \frac{d^3 r'}{r'^{2\gamma} |\vec{r} - \vec{r}'|^2} = \int \frac{d\Omega dr'}{r'^{2\gamma-2} |\vec{r} - \vec{r}'|^2} \propto \frac{1}{r^{2\gamma-1}}, \quad (22)$$

where the last relation follows just from dimensional analysis. Hence, the slope of the photon source term at $r \ll \lambda$ is reduced by one power with respect to $\rho^2(r)$. Since for a NFW profile $\gamma = 1$, we find for $r \ll \lambda$ that $\rho_{\text{eff}}(r) \propto \rho_{\text{NFW}}(r) \propto 1/r$. Note that for DM decay the source of gamma rays is proportional to $\rho(r)$, in contrast to the $\rho^2(r)$ for annihilations. Therefore, for a NFW profile our scenario exactly interpolates between DM decay at $r \ll \lambda$ and annihilation at $r \gg \lambda$. This behavior is shown in Fig. 2. Note that the parameter λ controls the absolute value of ρ_{eff}^2 at small r . For $\lambda \simeq 40$ kpc one would match exactly the profile for DM decay in the particular (somewhat arbitrary) normalization used in Fig. 2. However, for such large λ the asymptotic $\rho^2(r)$ behavior at large r is reached only at distances much larger than the size of our galaxy. We emphasize that the *slope* at small r is independent of λ , and hence it is a generic prediction of our scenario that for profiles with $\gamma \simeq 1$ at $r \lesssim r_{\odot}$ the gamma ray signal looks like DM decay from the inner region of the galaxy (cf. Eq. 15), whereas it mimics DM annihilation when looking away from the galactic center.

Let us now discuss the dependence of the J -factor, Eq. 19, on λ . In contrast to the usual annihilation case, J encodes not only the astrophysical DM profile, but it depends now also

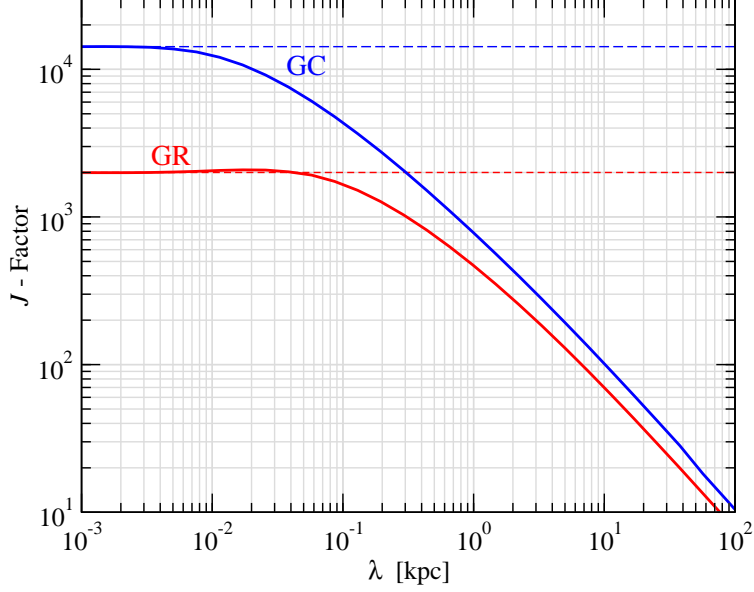


FIG. 3: J -factors for GC and GR as a function of λ . Dashed lines correspond to the J -factors for $\lambda = 0$.

on the particle physics parameter λ via ρ_{eff} . This dependence is shown in Fig. 3 for the GC and GR regions observed by HESS, see Eqs. 8 and 10. The figure shows that J gets reduced as soon as λ becomes larger than the size x of the observed region, since then most of the ϕ decay outside of the observed region. For the GC we have $x \simeq r_{\odot} \sqrt{\Delta\Omega_{\text{GC}}/\pi} \approx 15$ pc, whereas for the GR we have $x \simeq r_{\odot} \sqrt{\Delta l \Delta b} \approx 73$ pc, in agreement with the values of λ where the curves in Fig. 3 start to deviate from the J -factor for $\lambda = 0$. In Tab. I we give J for the GC and GR for some values of λ .

III. APPLICATION TO RECENT COSMIC RAY DATA

In this section we apply our LLP scenario to the recent data from cosmic ray experiments and discuss various other constraints. We describe our fit to the electron and positron data from PAMELA and ATIC in Sec. III A, and show that such a fit can be made consistent with the HESS GC and GR observations in Sec. III B. The bounds from neutrinos are discussed in Sec. III C.

A. The electron-positron signals

The electron flux from DM annihilations (which is equal to the positron flux) at r_{\odot} is calculated as

$$\frac{d\Phi_e}{dE_e} = \frac{v_e}{4\pi b(E_e)} \langle \sigma v \rangle \frac{\rho_{\text{eff}}^2(r_{\odot})}{m_{\chi}^2} \int_{E_e}^{m_{\chi}/2} dE' \frac{dN_e}{dE'} I(\lambda_D(E_e, E')), \quad (23)$$

with $b(E_e) = E_e^2/(\text{GeV} \tau_E)$, $\tau_E = 10^{16}$ s, and the electron velocity $v_e \approx c$. dN_e/dE is the injection spectrum for electrons (equal to the one for positrons) per ϕ decay, which we

λ [kpc]	global			PAMELA-only		
	m_χ [TeV]	$\langle\sigma v\rangle$ [cm^3s^{-1}]	χ^2_{\min}	m_χ [TeV]	$\langle\sigma v\rangle$ [cm^3s^{-1}]	χ^2_{\min}
0	3.3	1.1×10^{-22}	94.9	0.40	3.2×10^{-24}	7.3
1	3.3	1.1×10^{-22}	94.3	0.35	2.5×10^{-24}	7.1
10	3.3	0.9×10^{-22}	103.6	0.40	2.5×10^{-24}	8.0
100	3.2	4.9×10^{-22}	105.5	0.32	10×10^{-24}	7.9

TABLE II: Best fit values of m_χ and $\langle\sigma v\rangle$ for the global electron-positron data (PAMELA, ATIC, PPB-BETS, HESS) and the PAMELA-only fit, for some representative values of the ϕ decay length λ . We show also the χ^2 values at the best fit. The number of degrees of freedom is 61 for the global data and 10 for PAMELA-only.

calculate by assuming that ϕ decays into muons. Then dN_e/dE is calculated from the decay of the muons by using `pythia-6.4.19` [28] taking into account final state radiation. We provide analytic parameterizations of the injection spectra in Appendix A. The diffusion length λ_D is given by $\lambda_D^2(E, E') = 4K_0\tau_E(E^{\delta-1} - E'^{\delta-1})/(1 - \delta)$ with E, E' in GeV and throughout this work we assume the so-called MED propagation model from [29], where $K_0 = 0.0112 \text{ kpc}^2/\text{Myr}$ and $\delta = 0.70$. The halo function $I(\lambda_D)$ is obtained as a series of Bessel- and Fourier transforms of $\rho_{\text{eff}}^2(r)/\rho_{\text{eff}}^2(r_\odot)$, see [29]. Note that the flux in Eq. 23 is a factor 2 larger than in the case of $\chi\chi$ annihilations directly into muons, since we obtain 2 ϕ 's for each $\chi\chi$ annihilation, each of them giving a $\mu^+\mu^-$ pair.

We consider the measurement of the positron fraction $\Phi_{e^+}/(\Phi_{e^+} + \Phi_{e^-})$ from PAMELA [1], where we use only the 9 data points above 6.8 GeV where the effect of solar modulation is expected to be small. Then we use data on the sum of electrons and positrons ($\Phi_{e^+} + \Phi_{e^-}$) from ATIC-I, ATIC-II [2], PPB-BETS [30], and HESS [31]. For the latter we enlarge the error bars by a factor 3 in order to account for various uncertainties, such as energy scale. When we fit “PAMELA only” also the lowest three data points from ATIC are included in order to constrain the normalization of the background fluxes. For the astrophysical electron and positron background fluxes we use the parameterization from [32] for the fluxes from Galprop [33]. Following [34], these fluxes are multiplied by $C_{e^\pm}E^{\alpha_{e^\pm}}$, where in the fit we allow free normalization constants C_{e^\pm} and assume $\alpha_{e^\pm} = 0 \pm 0.05$ (1σ), independently for e^- and e^+ .

The results of our fit to electron data are shown as the shaded regions in Fig. 4 in the plane of the DM mass m_χ and the χ annihilation cross section $\langle\sigma v\rangle$ for four choices of the ϕ decay length λ . These regions are defined by contours of $\Delta\chi^2 = 11.8$ with respect to the χ^2 minimum (3σ for 2 dof). The corresponding best fit values are given in Tab. II, and the fit to the data is shown in Fig. 5.

The bump in the electron spectrum found by ATIC combined with the steep slope of the high-energy HESS data provides a strong constraint on the DM mass, since the peak of the electron spectrum, which occurs slightly below the threshold at $m_\chi/2$, has to match the bump in the data around 800 GeV. Therefore, if ATIC data are included m_χ is constrained to a narrow range around 3 TeV. If we fit only PAMELA data there is a degeneracy between m_χ and $\langle\sigma v\rangle$, and as long as the peak in the electron spectrum is above the last PAMELA data point at 83 GeV a good fit is obtained. As shown in Fig. 4 these results are basically

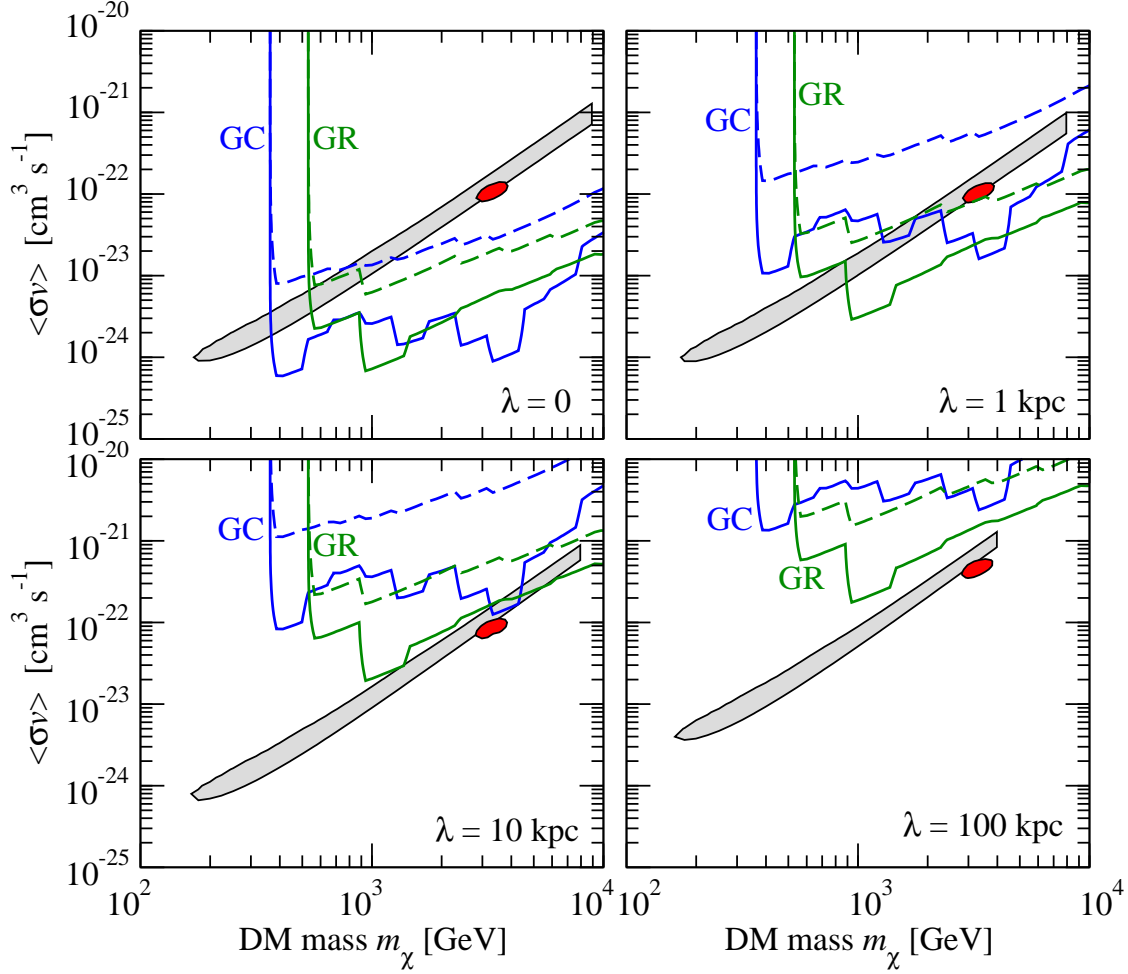


FIG. 4: Allowed regions at 3σ for PAMELA (gray) and PAMELA + electron-positron data (red) and the constraints from HESS photon observations of the galactic center (GC) and galactic ridge (GR) for $\lambda = 0, 1, 10, 100$ kpc. The solid (dashed) curves show HESS constraints at 90% CL with (at 3σ without) including a power law background in the fit, see text for details. The regions above the curves are excluded.

independent of the ϕ decay length λ , as long as this is not much larger than the distance from us to the center of the galaxy. The reason is that electrons and positrons are trapped in the turbulent galactic magnetic field and the observed signal is dominated by sources “near by”, within several kpc. Therefore, they are not very sensitive to the change of the source distribution from $\rho^2(r)$ to $\rho_{\text{eff}}^2(r)$, which is mostly important close to the galactic center. Only if λ becomes much larger than $r_\odot \approx 8.5$ kpc the total electron production close to us will be suppressed, which would require an increase in the annihilation cross section to maintain the signal. This effect is visible in Fig. 4 and Tab. II from the results for $\lambda = 100$ kpc.

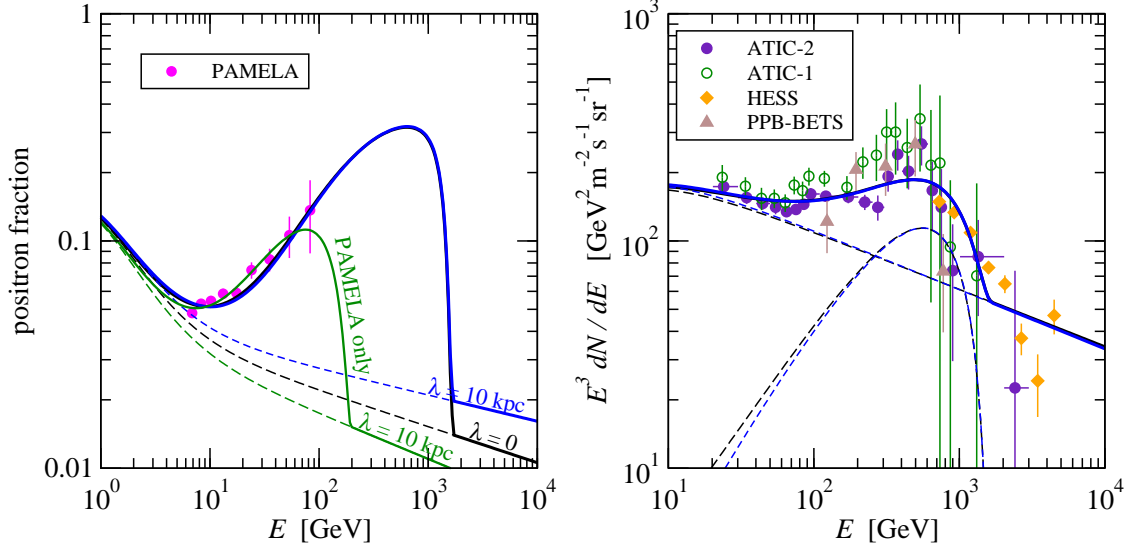


FIG. 5: PAMELA data on the positron fraction (left) and the electron-positron data (right) compared to the predicted spectra for $\lambda = 0$ (black curves) and $\lambda = 10$ kpc (blue curves) at the best fit values given in Tab. II. Solid curves correspond to signal + background, whereas with the dashed curves we show background and signal (right panel only) components separately. The green curve in the left plot shows the spectrum at the best fit to only PAMELA data for $\lambda = 10$ kpc.

B. Gamma ray constraints from HESS GC and GR observations

The photon fluxes predicted for given particle physics parameters $m_\chi, \langle\sigma v\rangle, \lambda$ by Eq. 18 can be compared with observations. We use the gamma ray data from HESS observations of the GC [17] and the GR [18]. These data range from about 200 GeV to 20 TeV and are consistent with a power law spectrum $\propto E_\gamma^{-\alpha}$ with $\alpha \approx 2.3$. In order to obtain bounds on DM parameters we adopt two different strategies. Most conservative bounds can be obtained by requiring that the signal predicted by DM must not exceed any data point of the observed flux. We obtain these bounds (denoted by “without background”) by excluding points in the parameter space where the prediction exceeds $x + 3\sigma$ for any data point, where x is the observed flux and σ its error bar. This leads to very conservative bounds, since it requires that in the signal region there is no astrophysical background, whereas in order to account for the observed flux at energies where DM does not contribute some astrophysical source has to be assumed. Therefore, we show also bounds by using a second method, called “with background”. Here we fit the data with a power law background (with free normalization and power) + the signal from DM. For given λ exclusion limits in the plane of m_χ and $\langle\sigma v\rangle$ at 90% CL are obtained by the contours with $\Delta\chi^2 = 4.6$ with respect to the χ^2 minimum. The photon spectrum dN_γ/dE_γ per ϕ decay used in Eq. 18 is calculated with `pythia-6.4.19` [28], assuming that ϕ decays into $\mu^+\mu^- + n\gamma$, see Appendix A.

The bounds from the HESS gamma ray observations are shown in Fig. 4 together with the regions favored by electron-positron data. Clearly, for $\lambda = 0$ the electron data are inconsistent with the gamma ray constraints. The photon flux from the galactic center gets reduced for finite λ , see Fig. 3, and the bounds shift to larger values of $\langle\sigma v\rangle$ as λ is increased. Fig. 4 shows that for $\lambda \simeq 10$ kpc the ATIC/PAMELA regions are consistent with the HESS

gamma ray constraints, even for the 90% CL bounds with background. As one might expect the bounds are also consistent with purely decaying dark matter [19, 35, 36] (and even in the case where decaying dark matter is also allowed to annihilate [37]). Both annihilating [38, 39, 40, 41] and decaying DM [42, 43, 44] may give rise also to a diffuse gamma ray signal observable (and partially already excluded) by FERMI/GLAST. For the LLP scenario we comment on this possibility in the Conclusions.

In addition to constraints from gamma rays, there are also strong constraints due to synchrotron radiation of radio waves. These bounds were extensively studied in [13, 15, 45, 46] where it was found that annihilation explanations of the positrons seem to be ruled out, unless the DM profiles are made effectively less steep as in decays or as in LLP. Thus it seems very plausible that for sufficiently large λ LLP can satisfy the bounds, though calculations along the lines of [13, 15] are in order. Constraints using potential gamma ray signals from dwarf galaxies, on the other hand, are less powerful [47, 48]. Constraints from galaxy clusters have been discussed in [49].

C. Neutrinos from the galactic center

Super-Kamiokande (SK) provides an upper limit on the upward going muon flux from various extra-terrestrial sources [50], see [51] for similar recent results from Ice Cube. Since the LLP scenario predicts 8 neutrinos for each DM annihilation (from the decay of the four muons from $\chi\chi \rightarrow \phi\phi \rightarrow 2\mu^+2\mu^-$) the bound on upward going muons from the galactic center is potentially relevant. The neutrino induced muon flux can be calculated as, see e.g. [52]

$$\Phi_\mu = \int_{E_{\text{thr}}}^{m_\chi/2} dE_\nu \frac{d\Phi_\nu}{dE_\nu} \int_{E_{\text{thr}}}^{E_\nu} dE_\mu R_\mu(E_\mu) \sum_{a=p,n} n_a \sum_{x=\nu,\bar{\nu}} \frac{d\sigma_x^a(E_\nu)}{dE_\mu}. \quad (24)$$

Here,

$$R_\mu(E_\mu) = \frac{1}{\rho\beta_\mu} \ln \frac{\alpha_\mu + \beta_\mu E_\mu}{\alpha_\mu + \beta_\mu E_{\text{thr}}} \quad (25)$$

is the range of a muon with energy E_μ until its energy drops below E_{thr} , for which we take the SK analysis threshold of 1.6 GeV, with $\alpha_\mu = 2 \times 10^{-3} \text{ GeV cm}^2 \text{ g}^{-1}$, $\beta_\mu = 4.2 \times 10^{-6} \text{ cm}^2 \text{ g}^{-1}$, and ρ is the density of the material in g cm^{-3} . Further, $n_a \approx r_a \rho / m_p$ are the number densities of neutrons and protons with $r_p \approx 5/9$, $r_n \approx 4/9$, and for the detection cross section we use

$$\frac{d\sigma_x^a(E_\nu)}{dE_\mu} \approx \frac{2m_p G_F^2}{\pi} \left(A_x^a + B_x^a \frac{E_\mu^2}{E_\nu^2} \right) \quad (26)$$

with $A_\nu^{n,p} = 0.25, 0.15$, $B_\nu^{n,p} = 0.06, 0.04$, and $A_{\bar{\nu}}^{n,p} = B_{\bar{\nu}}^{n,p}$, $B_{\bar{\nu}}^{n,p} = A_\nu^{p,n}$ [53].

$d\Phi_\nu/dE_\nu$ is the flux of muon neutrinos arriving at the earth within a solid angle $\Delta\Omega$. In our case the flux is equal for neutrinos and anti-neutrinos, and it is given by

$$\frac{d\Phi_\nu}{dE_\nu} = \frac{\langle \sigma v \rangle}{4\pi} \frac{r_\odot \rho_\odot^2}{m_\chi^2} \left(P_{\nu_e \rightarrow \nu_\mu} \frac{dN_{\nu_e}}{dE_\nu} + P_{\nu_\mu \rightarrow \nu_\mu} \frac{dN_{\nu_\mu}}{dE_\nu} \right) J \Delta\Omega. \quad (27)$$

The oscillation probabilities in terms of the lepton mixing matrix elements $U_{\alpha i}$ are $P_{\nu_e \rightarrow \nu_\mu} = \sum_{i=1}^3 |U_{ei}|^2 |U_{\mu i}|^2 \approx 0.21$, $P_{\nu_\mu \rightarrow \nu_\mu} = \sum_{i=1}^3 |U_{\mu i}|^4 \approx 0.395$. $dN_{\nu_e(\nu_\mu)}/dE_\nu$ is the spectrum of

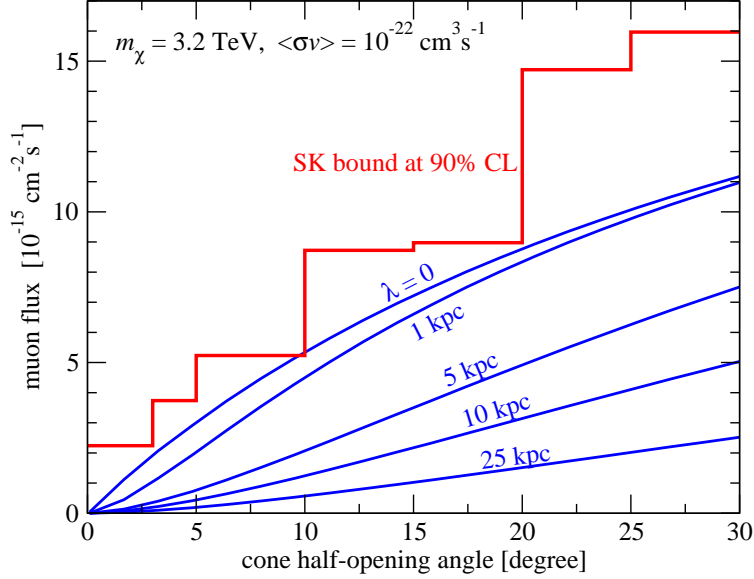


FIG. 6: Muon flux predicted for $m_\chi = 3.2$ TeV, $\langle\sigma v\rangle = 10^{-22} \text{ cm}^3/\text{s}$ and various values of λ , compared to the 90% CL upper limit from Super-Kamiokande [50].

electron (muon) neutrinos per ϕ decay (and integrates to 1). A parameterization for it is given in Appendix A. The J -factor in Eq. 27 is defined in the same way as for photons, see Eq. 19, and therefore the neutrino flux will be reduced with increasing the ϕ decay length λ similar to the case of photons.

SK provides an upper bound on the muon flux from a cone around the galactic center as a function of the cone half opening angle up to 30° . In Fig. 6 we compare the SK upper bound to the predicted muon fluxes for fixed m_χ and $\langle\sigma v\rangle$ as a function of λ . We conclude that $\lambda = 0$ is close to the present bound, while for $\lambda \gtrsim 5$ kpc the SK bound is significantly relaxed. For SK neutrino bounds for decaying DM see [54, 55, 56].

Let us also mention that in the LLP scenario we do not expect any observable neutrino flux from DM annihilations in the sun (or in the earth), since ϕ is to a very good approximation stable at the scale of the solar system. These neutrino fluxes will be exponentially suppressed by the ratio of the sun–earth distance (or the earth radius) to λ .

IV. CAN χ BE A THERMAL RELIC?

Let us now address the issue of whether or not χ can be a thermal relic. The LLP scenario, where χ annihilates first to 2 ϕ 's and these then after some time decay to SM particles, faces similar challenges as direct χ 's annihilation into SM particles.

First of all, for χ to be a thermal relic, the required χ annihilation cross section at the time of freeze-out in the early universe is several orders of magnitudes too small to explain the PAMELA/ATIC anomaly. For χ with TeV mass, the cross section at the freeze-out should be about $\langle\sigma v\rangle_{\text{FO}} \sim 3 \times 10^{-26} \text{ cm}^3 \text{ s}^{-1}$, while as we have seen in section III A, the annihilation cross section that explains the PAMELA/ATIC anomaly, is much larger, $\langle\sigma v\rangle_{\text{PA}} \sim 10^{-22} \text{ cm}^3 \text{ s}^{-1}$. One intriguing possibility which can explain the mismatch is that

there exists an attractive long range force between the dark matter particles [57]². This leads to an enhancement of the cross section at small velocities by a factor of $1/v$. With a typical velocity of χ 's in the galactic halo $v/c \sim 10^{-3}$ this so called ‘‘Sommerfeld enhancement’’ is roughly of the right size. In the LLP scenario for the case of a non-relativistic ϕ , there is a final phase space suppression of the cross section for χ 's annihilating in the galactic halo compared to the early universe. However, larger Sommerfeld enhancements are attainable, if there exists a bound state very close to threshold [58, 59].

The Sommerfeld enhancement solution has several potential phenomenological problems. For instance, if the Sommerfeld enhancement worked to arbitrarily small velocities, then annihilation in proto-halos could lead to a too large contribution to the diffuse gamma ray background [60]. For massive enough attractive force carriers this bound does not apply (such as GeV mass force carriers of [21]) as the enhancement saturates. More importantly, the highly energetic leptons and photons originating from χ annihilations at $T \lesssim 10$ keV in the early universe could lead to photo-dissociation of light elements destroying the successful predictions of standard big bang nucleosynthesis (BBN) [61]. The resulting bound on the annihilation cross section for $\chi\chi \rightarrow \mu^+\mu^-$ is $\langle\sigma v\rangle_{\text{FO}} < 2.0 \times 10^{-23} \text{ cm}^3\text{s}^{-1} \times (m_\chi/1 \text{ TeV})^{-1}$. This bound is already somewhat smaller than needed for the explanation of the PAMELA/ATIC anomaly, see Fig 4. The bound itself was obtained assuming time independent cross section, so a more detailed study in the framework of models giving Sommerfeld enhancement (and in the LLP scenario) may be warranted. However, since in our case ϕ is very long lived compared to BBN time scales, one may expect that within the LLP scenario there is no threat for BBN from rapid χ annihilations, while there are constraints from the late decays of ϕ 's, see below.

There are other ways to ‘‘boost’’ the annihilation cross section in the galactic halo without running into these phenomenological problems. For instance the annihilation could go through a resonance with mass of order $2m_\chi$ [62, 63]. This could arise naturally in models of extra dimensions with linearly spaced KK modes. Another possibility would be a kination model [64, 65], where the expansion rate at the time of decoupling is increased due to a rolling scalar field, leading to a reduced relic density. Yet another possibility is that χ is a product of a decay of a different meta-stable thermal relic [66]. Clearly, no boost factor is needed for decaying DM, but the large decay time leads to interesting model-building implications [55, 67, 68, 69].

In the LLP scenario, where χ is a thermal relic and ϕ a meta-stable thermal relic, there are other constraints coming from the late decay of the ϕ particle. Phenomenologically, the LLP scenario is interesting if ϕ travels a distance $\lambda \gtrsim 10$ kpc, because then it has a significant impact on the expected photon flux from the galactic center as discussed in section III B. This means that the ϕ life time is

$$\tau = \frac{\lambda}{c\beta\gamma} \simeq \frac{10^{12} \text{ s}}{\beta\gamma} \left(\frac{\lambda}{10 \text{ kpc}} \right). \quad (28)$$

Such late decaying relics can lead to modifications of the light element abundances [70, 71]. For TeV masses and lifetimes in this range, the ϕ particle must have a relic density which is three orders of magnitude smaller than the one for χ , see figures 5 and 6 of [71]. For

² Long range means here that the mass of the force carrier is smaller than Mv .

$\tau \gtrsim 10^{13}$ s there is an even stronger bound on the ϕ abundance due to constraints on the diffuse gamma ray background [70, 72] (see figure 7 of [72], where the bounds were derived for the case of radiative decays, while the bounds for leptonic decays are expected to be slightly weakened). The ratio $\sigma_{\chi}^{\text{ann}}/\sigma_{\phi}^{\text{ann}}$ must therefore be of order 10^{-3} or smaller. Consequently, if the couplings to quarks are not excessively suppressed, ϕ pair production should be observable at LHC. We leave it as an open exercise in model building to embed the above hierarchy of cross sections in a concrete model.

V. DISCUSSION AND CONCLUSIONS

In this paper we introduced a scenario for cosmic ray production due to dark matter (DM) which is an alternative to annihilations or decays³. The scenario softens the angular distribution of the gamma ray spectrum by having the DM annihilate into long lived particles (LLP), that subsequently decay to SM particles. We have demonstrated within the context of the PAMELA and ATIC positron and electron cosmic ray anomaly, that while standard DM annihilation scenarios seem to be in conflict with the gamma ray data due to large required cross sections ($\langle\sigma v\rangle \sim 10^{-23} \text{ cm}^3 \text{ s}^{-1}$), the prolongation of the final state lifetimes in the LLP scenario can accommodate the data. It should be emphasized that the gamma ray bounds are sensitive to the dark matter profiles. For less cuspy profiles the bounds would be weakened. Here we have only considered the NFW profile which grows as $1/r$ for small r . Recent simulations [73, 74] that include baryons seem to indicate an even faster rise for small r which would only strengthen the gamma ray bounds.

An attractive feature of DM annihilations is the direct relation between the annihilation cross section for indirect DM detection and the production cross section at collider experiments. In the LLP scenario this connection is lost to some extent, since the annihilation cross section of χ is not directly related to the production cross section of ϕ . However, assuming that χ and ϕ are thermal relics, bounds from light element abundances and diffuse gamma rays on decaying relics imply that the annihilation cross section of ϕ has to be some orders of magnitude larger than the one of χ in order to suppress its relic abundance, see discussion in section IV. Under the assumption of a non-negligible coupling to hadrons this implies good prospects for ϕ production at LHC (if kinematically accessible).

It is interesting to ask how one would differentiate the LLP scenario from DM decay. The FERMI satellite should be able to accurately measure the angular distribution of the gamma ray flux. This distribution can be used to differentiate between decays and the LLP scenario introduced in this paper. Figure 7 shows the gamma ray flux at fixed galactic latitude $b = 15$ degrees as a function of the galactic longitude for the decay and the annihilation profiles together with the one for the LLP scenario with $\lambda = 10$ kpc. We see that while the long lifetime reduces the slope compared to annihilation it still cuts off faster than the decay profile. An analysis of the angular distribution for decaying dark matter was performed in [35] and it would be interesting to extend this analysis to our scenario.

Another distinguishing feature of LLP will be the smearing out of clumps. If the only boost factor were due to clumps then this would be a striking signal for dark matter. Typi-

³ A scenario where the dark matter both annihilates and decays was proposed in [37].

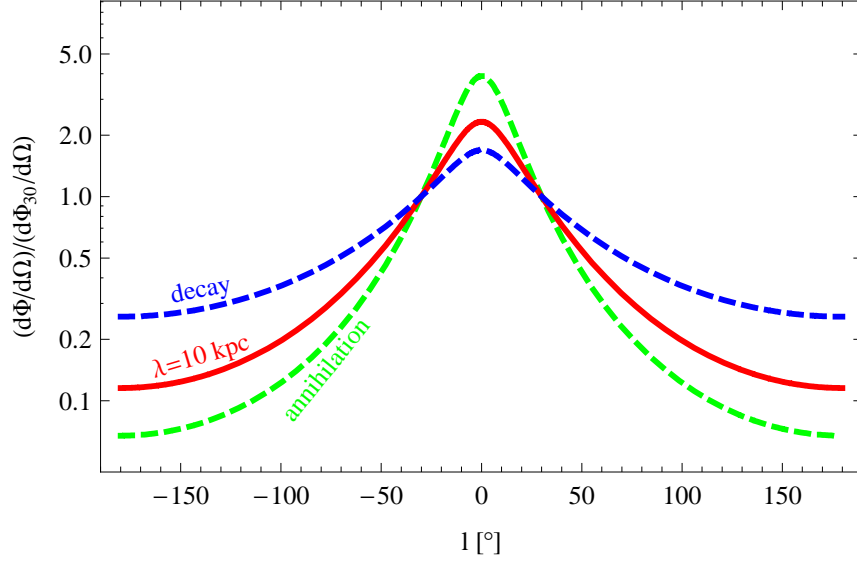


FIG. 7: Angular distribution of the gamma ray flux for the LLP scenario with $\lambda = 10$ kpc in comparison to the ones for DM decay and annihilation. We show the gamma ray flux for fixed galactic latitude $b = 15^\circ$ as a function of the longitude l , normalized to its value at 30° .

cally the over-densities lie towards the edges of galaxies where they are not tidally disrupted. The long lived particle scenario would smooth out this striking signal.

Finally, here we have explored only the case of non-relativistic intermediate states, which implies a near degeneracy between the DM and the LLP. However, the softening of the angular distribution demonstrated here, which allows one to avoid constraints from gamma ray bounds, should be active in the case of relativistic annihilation products as well. An investigation of this case is warranted.

Acknowledgement

T.S. acknowledges support from the Transregio Sonderforschungsbereich TR27 “Neutrinos and Beyond” der Deutschen Forschungsgemeinschaft.

APPENDIX A: INJECTION SPECTRA

Here we provide injection spectra for photons, electrons, and neutrinos resulting from the decay $\phi \rightarrow \mu^+ \mu^-$ in ϕ ’s rest frame.⁴ Since we work in the limit where ϕ ’s are non-relativistic, the provided injection spectra can be directly used in the numerical analysis in section III. The spectra are obtained by fitting analytic functions to a Monte Carlo sample generated with `pythia-6.4.19` [28]. In the following we define $x = 2E/m_\phi$ and $0 \leq x \leq 1$.

⁴ The spectra apply also for the case of standard annihilations $\chi\chi \rightarrow \mu^+ \mu^-$ by replacing $m_\phi \rightarrow 2m_\chi$.

Photon injection spectra. The photon spectrum for the decay (or similarly annihilation) of a heavy particle with mass m_ϕ into charged particles is well described by the Weizsäcker-Williams form (see e.g. [14, 15])

$$\frac{dN_\gamma}{dE_\gamma} = \frac{\alpha_{\text{em}}}{E_\gamma \pi} [(1-x)^2 + 1] \ln \left[\frac{m_\phi^2(1-x)}{m_l^2} \right]. \quad (\text{A1})$$

To be specific we have assumed here decay into a lepton pair l . Though in our work we consider only the muon final state we list here for completeness also the photon spectrum for electron and tau final states. The results from Pythia for muon and electron final states are very close to Eq. A1. In the range for E_γ from 10 GeV to 500 GeV for 1 TeV decaying DM the Pythia spectrum is 0.8 to 0.6 of the Weizsäcker-Williams form. We parameterize the spectrum by

$$\frac{dN_\gamma}{dE_\gamma} = A \frac{\alpha_{\text{em}}}{E_\gamma \pi} \left(\ln \left[\frac{m_\phi^2(1-x)}{m_l^2} \right] + B \right) [(1-x)^2 + C]. \quad (\text{A2})$$

The coefficients in the above formula depend on the value of m_ϕ . We parameterize this dependence by

$$K(m_\phi) = K_0 \left(\frac{m_\phi}{1 \text{ TeV}} \right)^{\delta_K}, \quad (\text{A3})$$

where $K = A, B, C$. Fitting Eq. A2 to the spectrum generated with Pythia we find for $m_\phi \in [10^2, 10^4]$ GeV:

$$\begin{aligned} e^+e^- \text{ final state: } & \begin{cases} (A_0, B_0, C_0) = (1.49197, -11.0576, 0.688768) \\ (\delta_A, \delta_B, \delta_C) = (0.050141, 0.235939, -0.00623121) \end{cases} , \\ \mu^+\mu^- \text{ final state: } & \begin{cases} (A_0, B_0, C_0) = (1.36693, -2.94774, 0.517128) \\ (\delta_A, \delta_B, \delta_C) = (-0.0365572, 0.412598, -0.0137187) \end{cases} . \end{aligned} \quad (\text{A4})$$

The photon spectrum is then described to better than 13% (18% for $\mu^+\mu^-$) everywhere in the fitted range (mostly to better than 5%). This was obtained from 6 values of m_ϕ , for each of the values with 10^7 simulated decay events.

For the decay into $\tau^+\tau^-$ we have produced 10^7 events in Pythia. Since the taus are heavy and can decay, producing hadrons and leptons, and these further decay or bremsstrahl photons, the Weizsäcker-Williams form Eq. A1 is no longer a good description of the final photon spectrum. A form that gives a good description is

$$\frac{dN_\gamma}{dE_\gamma} = A_0 \frac{\alpha_{\text{em}}}{E_\gamma \pi} \exp[-(A_1 x + A_2 x^2)] + \frac{B_0}{1 \text{ GeV}} + \frac{B_1}{1 \text{ GeV}} x, \quad (\text{A5})$$

with A_i, B_i depending as in Eq. A3 on m_ϕ with

$$\begin{aligned} (A_0^0, A_1^0, A_2^0, B_1^0, B_2^0) &= (283.066, -0.981786, 5.80398, -0.000155047, 0.000145457) \\ (\delta_{A_0}, \delta_{A_1}, \delta_{A_2}, \delta_{B_1}, \delta_{B_2}) &= (0.00118045, -0.0141779, -0.00573809, -0.966239, -0.964131) \end{aligned} \quad (\text{A6})$$

The error on the predicted spectra is below 15% (in the first bin it is 30%).

Electron injection spectra. Consider a two-body decay $\phi \rightarrow \mu^+ \mu^-$ and neglect the photon emission. Then the electron spectrum can be obtained by boosting the isotropic spectrum from the muon rest frame into the rest frame of ϕ . In our work we do include final state radiation and therefore, we prefer to use the electron spectrum generated with Pythia. We use the function

$$\frac{dN_e}{d(E_e/1 \text{ GeV})} = A_0 \frac{\alpha_{\text{em}}}{\pi} \exp[-(A_1 x + A_2 x^2)] + B_0 + B_1 x, \quad (\text{A7})$$

with A_i, B_i depending as in Eq. A3 on m_ϕ . Fitting this form to the generated spectrum we find

$$\begin{aligned} (A_0^0, A_1^0, A_2^0, B_0^0, B_1^0) &= (-0.296635, 2.65121, 14.8445, 0.0042505, -0.00427157) \\ (\delta_{A_0}, \delta_{A_1}, \delta_{A_2}, \delta_{B_0}, \delta_{B_1}) &= (-1.01424, 0.017198, -0.0107585, -0.999819, -0.999819). \end{aligned} \quad (\text{A8})$$

The error on the predicted spectra is below 7%.

Neutrino injection spectra. In each decay $\phi \rightarrow \mu^+ \mu^-$ we have two neutrinos— ν_μ and ν_e —and two antineutrinos with the same spectra. It turns out to be convenient to fit for the full neutrinos spectrum ($\nu_e + \nu_\mu$) and for the electron neutrino spectrum separately. The muon neutrino spectrum is then the difference between the total neutrino spectrum and the electron neutrino spectrum. For the total $\nu_e + \nu_\mu$ neutrino spectrum (normalized to 2) we use the parameterization

$$\frac{dN_\nu}{d(E_\nu/1 \text{ GeV})} = A_0 \frac{\alpha_{\text{em}}}{\pi} \exp[-(A_1 x + A_2 x^2)] + B, \quad (\text{A9})$$

with A_i, B depending as in Eq. A3 on m_ϕ and

$$\begin{aligned} (A_0^0, A_1^0, A_2^0, B^0) &= (3.73892, 0.0128514, 2.0015, -0.00117002) \\ (\delta_{A_0}, \delta_{A_1}, \delta_{A_2}, \delta_B) &= (-1.0019, -0.283851, 0.00350415, -1.01054) \end{aligned} \quad (\text{A10})$$

with the error on the predicted spectra below 4% (but mostly below 2%). And for the electron neutrino spectrum we use

$$\frac{dN_\nu}{d(E_\nu/1 \text{ GeV})} = A_0 \frac{\alpha_{\text{em}}}{\pi} \exp[-(A_1 x + A_2 x^2 + A_{1/2} \sqrt{1-x})] + B, \quad (\text{A11})$$

with again A_i, B depending as in Eq. A3 on m_ϕ , and

$$\begin{aligned} (A_0^0, A_1^0, A_2^0, B^0, A_{1/2}^0) &= (14.4735, 0.90821, 2.90886, -0.000653652, 1.95634) \\ (\delta_{A_0}, \delta_{A_1}, \delta_{A_2}, \delta_B, \delta_{A_{1/2}}) &= (-0.994217, -0.00194938, 0.00048921, -0.985772, -0.000395335) \end{aligned} \quad (\text{A12})$$

The ν_e spectrum is described to better than 5%.

[1] O. Adriani *et al.*, arXiv:0810.4995 [astro-ph].

[2] J. Chang *et al.*, Nature **456** (2008) 362.

- [3] A. Buffington, C. D. Orth and G. F. Smoot, *Astrophys. J.* **199**, 669 (1975); D Mueller and K.K Tang, *Astrophys. J.* **312**, 183 (1987); R. L. Golden *et al.*, *Astrophys. J.* **436**, 769 (1994); S. W. Barwick *et al.* [HEAT Collaboration], *Astrophys. J.* **482**, L191 (1997) [arXiv:astro-ph/9703192].
- [4] S. Torrii *et al.*, *Astrophys. J.* **559**, 973 (2001); J. Nishimura *et al.*, *Advances in Space Research* **19**, 767 (1997); J. Nishimura *et al.* *Astrophys. J.* **238**, 394 (1980).
- [5] J. H. Taylor and D. R. Stinebring, *ARA&A* **24**, 285 (1986).
- [6] D. C. Backer, *Pulsars* (Galactic and Extragalactic Radio Astronomy, 1988), pp. 480521. (2008).
- [7] D. Hooper, P. Blasi and P. D. Serpico, *JCAP* **0901**, 025 (2009) [arXiv:0810.1527 [astro-ph]].
- [8] H. Yuksel, M. D. Kistler and T. Stanev, arXiv:0810.2784 [astro-ph].
- [9] S. Profumo, arXiv:0812.4457 [astro-ph].
- [10] N. J. Shaviv, E. Nakar and T. Piran, arXiv:0902.0376 [astro-ph.HE].
- [11] D. Malyshev, I. Cholis and J. Gelfand, arXiv:0903.1310 [astro-ph.HE].
- [12] J. Hall and D. Hooper, arXiv:0811.3362 [astro-ph].
- [13] G. Bertone, M. Cirelli, A. Strumia and M. Taoso, arXiv:0811.3744 [astro-ph].
- [14] N. F. Bell and T. D. Jacques, arXiv:0811.0821 [astro-ph].
- [15] L. Bergstrom, G. Bertone, T. Bringmann, J. Edsjo and M. Taoso, arXiv:0812.3895 [astro-ph].
- [16] P. Meade, M. Papucci and T. Volansky, arXiv:0901.2925 [hep-ph].
- [17] F. Aharonian *et al.* [H.E.S.S. Collaboration], *Phys. Rev. Lett.* **97**, 221102 (2006) [Erratum-*ibid.* **97**, 249901 (2006)] [arXiv:astro-ph/0610509].
- [18] F. Aharonian *et al.* [H.E.S.S. Collaboration], *Nature* **439**, 695 (2006) [arXiv:astro-ph/0603021].
- [19] E. Nardi, F. Sannino and A. Strumia, *JCAP* **0901** (2009) 043 [arXiv:0811.4153 [hep-ph]].
- [20] M. Pospelov and A. Ritz, *Phys. Lett. B* **671**, 391 (2009) [arXiv:0810.1502 [hep-ph]].
- [21] N. Arkani-Hamed, D. P. Finkbeiner, T. Slatyer and N. Weiner, *Phys. Rev. D* **79**, 015014 (2009) [arXiv:0810.0713 [hep-ph]].
- [22] I. Cholis, D. P. Finkbeiner, L. Goodenough and N. Weiner, arXiv:0810.5344 [astro-ph].
- [23] Y. Nomura and J. Thaler, arXiv:0810.5397 [hep-ph].
- [24] I. Cholis, G. Dobler, D. P. Finkbeiner, L. Goodenough and N. Weiner, arXiv:0811.3641 [astro-ph].
- [25] P. J. Fox and E. Poppitz, arXiv:0811.0399 [hep-ph].
- [26] J. Mardon, Y. Nomura, D. Stolarski and J. Thaler, arXiv:0901.2926 [hep-ph].
- [27] J. F. Navarro, C. S. Frenk and S. D. M. White, *Astrophys. J.* **462**, 563 (1996) [arXiv:astro-ph/9508025].
- [28] T. Sjostrand, S. Mrenna and P. Skands, *JHEP* **0605**, 026 (2006) [arXiv:hep-ph/0603175].
- [29] T. Delahaye, R. Lineros, F. Donato, N. Fornengo and P. Salati, *Phys. Rev. D* **77** (2008) 063527 [arXiv:0712.2312 [astro-ph]].
- [30] S. Torrii *et al.*, arXiv:0809.0760 [astro-ph].
- [31] F. Aharonian *et al.* [H.E.S.S. Collaboration], *Phys. Rev. Lett.* **101**, 261104 (2008) [arXiv:0811.3894 [astro-ph]].
- [32] E. A. Baltz and J. Edsjo, *Phys. Rev. D* **59**, 023511 (1999) [arXiv:astro-ph/9808243].
- [33] I. V. Moskalenko and A. W. Strong, *Astrophys. J.* **493** (1998) 694 [arXiv:astro-ph/9710124].
- [34] M. Cirelli, R. Franceschini and A. Strumia, *Nucl. Phys. B* **800**, 204 (2008) [arXiv:0802.3378 [hep-ph]].

- [35] G. Bertone, W. Buchmuller, L. Covi and A. Ibarra, JCAP **0711**, 003 (2007) [arXiv:0709.2299 [astro-ph]].
- [36] A. Ibarra and D. Tran, arXiv:0811.1555 [hep-ph].
- [37] K. Cheung, P. Y. Tseng and T. C. Yuan, arXiv:0902.4035 [hep-ph].
- [38] C. R. Chen, M. M. Nojiri, S. C. Park, J. Shu and M. Takeuchi, arXiv:0903.1971 [hep-ph].
- [39] E. Borriello, A. Cuoco and G. Miele, arXiv:0903.1852 [astro-ph.GA].
- [40] M. Lattanzi and J. I. Silk, arXiv:0812.0360 [astro-ph].
- [41] R. Harnik and G. D. Kribs, arXiv:0810.5557 [hep-ph].
- [42] K. Ishiwata, S. Matsumoto and T. Moroi, arXiv:0903.0242 [hep-ph].
- [43] S. Shirai, F. Takahashi and T. T. Yanagida, arXiv:0902.4770 [hep-ph].
- [44] P. Grajek, G. Kane, D. Phalen, A. Pierce and S. Watson, arXiv:0812.4555 [hep-ph].
- [45] J. Zhang, X. J. Bi, J. Liu, S. M. Liu, P. f. Yin, Q. Yuan and S. H. Zhu, arXiv:0812.0522 [astro-ph].
- [46] K. Ishiwata, S. Matsumoto and T. Moroi, Phys. Rev. D **79**, 043527 (2009) [arXiv:0811.4492 [astro-ph]].
- [47] R. Essig, N. Sehgal and L. E. Strigari, arXiv:0902.4750 [hep-ph].
- [48] L. Pieri, M. Lattanzi and J. Silk, arXiv:0902.4330 [astro-ph.HE].
- [49] Q. Yuan, X. Bi, F. Huang and X. Chen, arXiv:0902.4294 [astro-ph.CO].
- [50] S. Desai *et al.* [Super-Kamiokande Collaboration], Phys. Rev. D **70**, 083523 (2004) [Erratum-ibid. D **70**, 109901 (2004)] [arXiv:hep-ex/0404025].
- [51] R. Abbasi, arXiv:0902.2460 [astro-ph.CO].
- [52] C. Delaunay, P. J. Fox and G. Perez, arXiv:0812.3331 [hep-ph].
- [53] V. Barger, W. Y. Keung, G. Shaughnessy and A. Tregre, Phys. Rev. D **76**, 095008 (2007) [arXiv:0708.1325 [hep-ph]].
- [54] J. Hisano, M. Kawasaki, K. Kohri and K. Nakayama, arXiv:0812.0219 [hep-ph].
- [55] A. Arvanitaki, S. Dimopoulos, S. Dubovsky, P. W. Graham, R. Harnik and S. Rajendran, arXiv:0812.2075 [hep-ph].
- [56] J. Liu, P. f. Yin and S. h. Zhu, arXiv:0812.0964 [astro-ph].
- [57] J. Hisano, S. Matsumoto, M. Nagai, O. Saito and M. Senami, Phys. Lett. B **646**, 34 (2007) [arXiv:hep-ph/0610249].
- [58] J. D. March-Russell and S. M. West, arXiv:0812.0559 [astro-ph].
- [59] M. Pospelov, A. Ritz and M. B. Voloshin, Phys. Lett. B **662**, 53 (2008) [arXiv:0711.4866 [hep-ph]].
- [60] M. Kamionkowski and S. Profumo, Phys. Rev. Lett. **101**, 261301 (2008) [arXiv:0810.3233 [astro-ph]].
- [61] J. Hisano, M. Kawasaki, K. Kohri, T. Moroi and K. Nakayama, arXiv:0901.3582 [hep-ph].
- [62] M. Ibe, H. Murayama and T. T. Yanagida, arXiv:0812.0072 [hep-ph].
- [63] W. L. Guo and Y. L. Wu, arXiv:0901.1450 [hep-ph].
- [64] P. Salati, Phys. Lett. B **571**, 121 (2003) [arXiv:astro-ph/0207396].
- [65] F. Rosati, Phys. Lett. B **570**, 5 (2003) [arXiv:hep-ph/0302159].
- [66] M. Fairbairn and J. Zupan, arXiv:0810.4147 [hep-ph].
- [67] M. Pospelov and M. Trott, arXiv:0812.0432 [hep-ph].
- [68] P. f. Yin, Q. Yuan, J. Liu, J. Zhang, X. j. Bi and S. h. Zhu, Phys. Rev. D **79**, 023512 (2009) [arXiv:0811.0176 [hep-ph]].

- [69] C. R. Chen, M. M. Nojiri, F. Takahashi and T. T. Yanagida, arXiv:0811.3357 [astro-ph].
- [70] J. R. Ellis, G. B. Gelmini, J. L. Lopez, D. V. Nanopoulos and S. Sarkar, Nucl. Phys. B **373**, 399 (1992).
- [71] M. Kawasaki and T. Moroi, Astrophys. J. **452**, 506 (1995) [arXiv:astro-ph/9412055].
- [72] G. D. Kribs and I. Z. Rothstein, Phys. Rev. D **55**, 4435 (1997) [Erratum-ibid. D **56**, 1822 (1997)] [arXiv:hep-ph/9610468].
- [73] O. Y. Gnedin, A. V. Kravtsov, A. A. Klypin and D. Nagai, Astrophys. J. **616**, 16 (2004) [arXiv:astro-ph/0406247].
- [74] S. Kazantzidis *et al.*, Astrophys. J. **623**, L67 (2005) [arXiv:astro-ph/0407407].